

Imprints of $U_A(1)$ chiral anomaly and disorder in the Dirac eigenspectrum of QCD at finite temperature

Ravi Shanker,^{1,2,*} Harshit Pandey,^{1,2} and Sayantan Sharma^{1,2}

¹*The Institute of Mathematical Sciences, Chennai 600113, India*

²*Homi Bhabha National Institute, Training School Complex, Anushaktinagar, Mumbai 400094, India*

We perform a comprehensive study of the properties of Dirac eigenvalue spectrum in QCD as a function of temperature on the lattice. In addition to effects due to interplay between interactions and disorder inherently present in a many-body system, the Dirac spectrum also contains crucial information about the effective restoration of different subgroups of almost exact two-flavor chiral symmetry in QCD. We calculate the infrared eigenvalues of the overlap Dirac operator on 2+1 flavor QCD ensembles generated using domain wall fermion discretization, on a large volume lattice. From the normalized level spacing ratios, we identify those eigenvalues that have intermediate level statistics, distinctly different from the majority in the bulk spectrum that follow universal level fluctuations similar to a random matrix of Gaussian unitary type. We provide an explanation of these intermediate level ratios in terms of a specific random matrix model and quantify the correlation between these eigenstates and disorder in the gauge fields manifested in the renormalized Polyakov loop values. Whereas the existence of *intermediate* eigenmodes is intimately connected to the *effective* restoration of different subgroups of chiral symmetry close to chiral crossover transition, their origin can be traced to random uncorrelated disorder at higher temperatures when the $U_A(1)$ is *effectively restored*. We also, for the first time, calculate the Thouless conductance for the Dirac spectrum that quantifies the structural rigidity of the eigenvectors, and use it as a diagnostic tool to understand the restoration of the anomalous $U_A(1)$ subgroup of chiral symmetry and localization driven by disorder.

PACS numbers: 12.38.Gc, 11.15.Ha, 11.30.Rd, 11.15.Kc

I. INTRODUCTION

Interacting many-body quantum systems continue to challenge our understanding of fundamental processes like thermalization and transport. Understanding the universal properties of the eigenvalue spectra of the Hamiltonians describing such systems provides valuable insights into their dynamics. The universal fluctuations of the level spacings between adjacent energy eigenvalues are one such observable. Bohigas-Giannoni-Schmit conjecture [1] states that for quantum systems whose classical dynamics is non-integrable, the universal fluctuations of the level separations between eigenvalues of the Hamiltonian belong to one of the three universality classes of Wigner-Dyson statistics within Random Matrix theory (RMT). On the other hand, if the corresponding classical dynamics is completely integrable, then the quantum energy eigenvalues behave like a sequence of independent random variables according to the Berry-Tabor conjecture [2]. Therefore, studying the universal level spacing fluctuations of a quantum system allows us to learn about the classical dynamics and vice versa, in particular, it enables us to understand how classical (non-)integrability manifests itself in the quantum many-body theory. This is important since it is expected that the long-time dynamics in classical non-integrable many-body systems, characterized by ergodicity and mixing in the phase space, is universally governed by a thermal

fixed point. However, the connection between chaos and thermalization is not very apparent in a quantum system [3].

Many realistic physical systems far from integrability exhibit quasi-periodic motion which is challenging to understand even from a purely classical point of view, let alone understanding the classical-quantum correspondence in these systems [4]. Some ideas inspired by semiclassical correspondence have been put forward by Berry and Robnik, who proposed that the spectral statistics of such mixed systems should be understood as arising from an uncorrelated superposition of spectra from different universality classes, each spectrum being associated with chaotic or regular regions in the classical phase space [5]. However, extensive investigations [4, 6, 7] reveal that the universal fluctuations of the energy spectrum characterized in terms of integrable (ordered) as well as non-integrable (disordered) regions might be correlated, even in cases where no classical analog might exist [8–13] or the ordered (integrable) spectra may become chaotic due to strong admixture. There can be other non-trivial scenarios as well. Many-body systems can undergo localization transitions when symmetries of the Hamiltonian are broken as a function of external parameters, e.g., the strength of disorder, leading to a change in the nature of level fluctuations. Such cases are typically addressed by random matrix ensembles which interpolate between Poisson and Wigner-Dyson level statistics as observed in localization transitions, e.g., close to the mobility edge [14] in the Anderson model [15]. In this particular case, the critical eigenstates for very closely

* Corresponding author: rshanker@imsc.res.in

spaced eigenvalues are strongly correlated and have significant overlap with each other in spite of their sparse fractal-like structure. However, very small correlations exist between eigenvalues with large separations.

A prominent example of a strongly interacting many-body quantum system, which has all these features, is described by a non-Abelian gauge theory known as Quantum Chromodynamics (QCD). The QCD Hamiltonian is difficult to realize in three dimensions (see e.g., Ref. [16] and references therein); instead, we study the spectral properties of the QCD Dirac operator in Euclidean 3+1 dimensions. The Dirac eigenspectrum consisting of eigenstates with different amounts of localization not only determines the transport properties in QCD but also explains key features of a non-trivial thermodynamic chiral crossover transition [17, 18] which is an exact phase transition in the chiral limit. Thus, a strongly interacting many-body system described by QCD is an important example of a theorist's laboratory to study how, in addition to the interplay between disorder and interactions, the correlations due to the criticality related to the chiral phase transition get imprinted in the level spacing statistics of the Dirac eigenvalues. This present work is a detailed study of the QCD Dirac spectrum which provides new insights and ways to disentangle the features due to changes in the localization (transport) properties as a function of temperature from those due to spontaneous breaking of different subgroups of chiral symmetry.

II. BACKGROUND

The eigenvalue spectrum of the Dirac operator provides important insights regarding the symmetries of QCD and their breaking. An eigenstate of the Dirac operator describes a one-particle massless fermion (quark) state in presence of a gauge background. The gauge fields provide both the interactions and the disorder whose strength varies as a function of temperature. Properties of the eigenvalue spectrum of the QCD Dirac operator, in presence of gauge ensembles, have been studied extensively using lattice QCD at zero as well as finite temperatures. The density of vanishingly small eigenvalues of the Dirac operator in the chiral symmetry broken phase gives an accurate estimate of the chiral condensate, the order parameter of the chiral phase transition in the limit of massless quarks [19]. At temperatures $T < T_{pc}$, where $T_{pc} \sim 156.5$ MeV is the pseudo-critical temperature [20–22] corresponding to the chiral crossover transition in QCD with physical quark flavors, the level statistics of the deep infrared part of the spectrum can be explained within the universality class of RMT consisting of chiral Gaussian unitary ensemble (GUE) [23–26] whereas for the higher eigenvalues the universal features can be explained within Wigner's classification with a RMT ensemble of conventional Gaussian unitary type.

At higher temperatures, the non-singlet part of the almost exact two-flavor chiral symmetry is *effectively* re-

stored, i.e. the disconnected part of the chiral susceptibility matches with the topological susceptibility up to $\mathcal{O}(m^2)$, where m is the mass of the light quark flavor [27, 28]. This also leads to perceptible changes in the eigenvalue spectrum of the Dirac operator—the intercept vanishes, leading to the formation of a small peak-like feature in the infrared part of the eigenvalue spectrum. This peak has been observed in studies using a mixed-action set-up [29–31] which was debated for a while [32–35]. However, existence of the peak-like feature was shown with dynamical domain wall fermions [36] on a finite lattice, now also observed to survive in the continuum limit in 2+1 QCD with HISQ discretization [37]. The higher (bulk) eigenvalues denoted by λ whose density grows linearly with λ are disordered i.e., their level spacing ratios are consistent with the predictions from RMT belonging to the GUE. The peak-like feature and bulk spectrum overlap strongly, resulting in the most infrared eigenmodes to be delocalized [38–40] but not ergodic, since their inverse participation ratio does not scale inversely with volume. Their level spacing fluctuations are intermediate between the Poissonian and GUE values [41]. These infrared eigenmodes are characteristic of a strongly-coupled regime [38, 42, 43] and exhibit fractal-like features [41]. The median of the distribution of fractal dimensions for these *intermediate* eigenvalues is tantalizingly similar to the expectations from an $O(4)$ spin model [41]. In contrast, bulk eigenstates are ergodic since their inverse participation ratios scale as $\sim L^{-2.8}$ [41] and are thus delocalized over the entire volume.

The $U_A(1)$ subgroup will be *effectively* restored at a temperature, $T_{U(1)}$, when physical observables which are sensitive to it, e.g., the topological susceptibility has a temperature dependence which is consistent with the expectation from a dilute gas of instantons. This can be motivated by the fact that once an onset to the dilute instanton gas regime occurs, there are no further changes in the topological properties even when temperatures are increased to asymptotically large values. The $T_{U(1)}$ is close to $\gtrsim 1.5 T_{pc}$ inferred from the temperature dependence of the topological susceptibility in QCD [27], from the features in the Dirac eigenvalue spectrum [29, 40], from the degeneracy of temporal meson correlators [44] and through tensor singlet channels [45]. A weaker bound $T_{U(1)} \gtrsim 1.2 T_{pc}$ was obtained from the fact that values of $\chi_\pi - \chi_\delta$ arising due to the mixing between near-zero eigenvalues with the bulk vanishes at this temperature [37].

The scenario at even higher temperatures $T > T_{U(1)}$ is not yet well understood. Whereas a peak-like feature of near-zero eigenmodes similar to $m^2\delta(\lambda)$ should survive, expected from a dilute gas-like scenario for instantons [29, 40, 46, 47], it is heavily suppressed as a function of temperature. Thus its contribution to topological susceptibility decreases as $\sim T^{-8}$ [27, 48, 49]. Eventually, these infrared modes should be gapped out from the bulk part of the eigenvalue spectrum. Recent studies indicate that at sufficiently high temperatures, the most infrared

part of this bulk spectrum contains localized eigenvalues which can be distinguished from the other delocalized bulk eigenmodes, which follow GUE level statistics, through a mobility edge [31, 50, 51]. This phenomenon is analogous to a localization transition [31, 51–56] observed in the Anderson model [15]. Nonetheless, a naive Anderson-like scaling of its temperature dependence demonstrates that the mobility edge might vanish at the pseudo-critical temperature [31, 52, 57], but it might also disappear only at the critical temperature which is achieved in the chiral limit [51]. The robustness of these observations will in the future be tested through carefully performed infinite volume and continuum extrapolations.

To summarize, whereas there is a wealth of results on spectral signatures related to *effective* restoration of the different subgroups of chiral symmetry, and on the localization properties akin to an Anderson-like transition, separately, the interplay between these two physically distinct phenomena is not so clear. We want to emphasize here that these two phenomena have distinct physical origins and thus their consequences will also be different. Anderson transition is a quantum phase transition which, strictly speaking, is a zero-temperature phenomenon. A possible way to understand such a (de)-localization transition at finite temperatures is to attribute the change in the strength of the disorder due to gauge fluctuations arising due to the change in temperature; however, a clear connection between the two is not very apparent. In QCD, varying the temperature also results in the sequential (effective) restoration of different subgroups of chiral symmetry. Evidence suggests that the restoration of the $SU_A(2)$ occurs through a second-order phase transition in the chiral limit [58], remnant effects of which will remain manifest in the Dirac eigenvalue spectrum even for physical light quarks [41]. The effective restoration of $U_A(1)$ will result in characteristic changes in the localization properties of the Dirac eigenvectors; on the other hand, an Anderson-like transition also results in structural changes in the eigenvectors of Dirac operator. It is thus imperative to disentangle these two phenomena, to unambiguously identify the mechanism that drives these effects. However, the temperature regimes where these occur overlap with each other which makes it challenging to unambiguously separate these two effects.

III. AN OUTLINE OF THIS WORK

In this work, we provide a systematic way of disentangling the impact of *effective* restoration of $U_A(1)$ from the gradual onset of localization driven by disorder in 1-particle quark states through a detailed study of the QCD Dirac eigenspectrum on the lattice. Though both these distinct physical phenomena result in the presence of infrared eigenvalues with intermediate level ratios at temperatures above T_{pc} , we discuss discerning observables that can distinguish between the two. We demonstrate

that the onset of localization at high temperatures due to disorder is distinct from the localization largely driven by topological fluctuations just above T_{pc} and can only be observed when the $U_A(1)$ subgroup of chiral symmetry is *effectively* restored.

We also measure for the first time the structural rigidity of the Dirac eigenstates in terms of its curvature arising as a result of applying a twist on one of the spatial boundaries of the lattice box. It is well known that the curvature of eigenvalues of the Hamiltonian is related to the Thouless conductance [59]. We propose that the analogue of Thouless conductance for the Dirac eigenspectrum can be used as a diagnostic tool for characterizing the *effective* restoration of $U_A(1)$.

IV. DETAILS ABOUT THE NUMERICAL TECHNIQUES

The gauge configurations for QCD with two light and a strange quark flavor were generated using Möbius domain wall discretization for fermions and Iwasaki gauge action. The computations were performed on a space-time lattice which has $N = 32$ sites along each of the three spatial directions and $N_\tau = 8$ sites along the Euclidean temporal direction. We focus on the high temperature phase where the non-singlet part of the (almost) exact two-flavor chiral symmetry in QCD is *effectively* restored, whereas its $U_A(1)$ subgroup remains broken but the magnitude of this breaking has a characteristic dependence on the temperature. At temperatures $T = 164\text{--}339$ MeV, we study the spectral properties of the QCD Dirac operator, realized on the lattice with the overlap Dirac operator. The gauge configurations for $T \lesssim 181$ MeV were already generated and used for calculating the disconnected piece of the chiral susceptibility and the pseudo-critical temperature $T_{pc} \simeq 158.7$ MeV [28]. The temperatures $T = 1/(N_\tau a)$ in physical units are expressed in terms of the Sommer parameter r_0 at each value of the gauge coupling g by relating it to the lattice spacing a through the two-loop beta-function [60]. However all gauge ensembles characterized by the bare parameter $\beta = 6/g^2$ for $\beta \gtrsim 1.829$ were generated from scratch. The temperature corresponding to $\beta = 1.829$ was already estimated in Ref. [60]. For precisely determining the temperature in MeV units for the larger β values, we have first extracted the lattice spacing a in units of the mass of the omega baryon m_Ω [60–62] for a wide range of $\beta = 1.70\text{--}2.31$. We next performed a fit of these extracted inverse spacings as a function of β and then used this fit and the 2-loop beta function to extract the corresponding temperatures in MeV for all β values. We checked that the temperature we extracted from this fit, corresponding to a lower $\beta = 1.633$, matches the value reported earlier [63]. Details of the parameters used in the configuration generation, e.g. the Möbius parameter c_5 , the extent of the fifth dimension L_5 and the number of eigenvalues computed for each statistically independent

configuration at different temperatures are mentioned in Table. I. The quark masses are physical which are fixed by setting the value of the pion mass to 140 MeV and kaon mass to 435 MeV [28]. The spatial lattice size in physical units varies between 4-2.5 fm for $T = 195$ -339 MeV.

As mentioned in Table I, we typically calculate the first 100-200 non-zero eigenvalues of $D_{ov}D_{ov}^\dagger$, where D_{ov} is the massless overlap Dirac operator on each of these gauge configurations. This choice of the lattice Dirac operator is motivated by the fact that the overlap fermions have an exact chiral symmetry on the lattice, satisfy an index theorem and do not have additional lattice artifacts due to the breaking of chiral symmetry, as in the case of Wilson fermions or the breaking of the continuum spin and flavor symmetries in staggered fermions. We have numerically implemented the overlap Dirac operator by representing the matrix sign function exactly in terms of the first 30 eigenvalues of $D_w^\dagger D_w$ and approximating it by a Zolotarev rational polynomial with 25 terms in the rest of the vector space. The numerical accuracy of our procedure ensures that the resultant overlap Dirac operator satisfies the Ginsparg-Wilson relation to a precision of $\lesssim 10^{-9}$ on each gauge configuration we have studied and the sign function is implemented to a numerical precision of 10^{-10} . The eigenvalues of the overlap Dirac operator are calculated numerically using the Kalkreuter-Simma Ritz algorithm [64] with restarts. For optimization, we have first estimated the number and chirality of zero modes present per configuration and used this information to project the $D_{ov}D_{ov}^\dagger$ onto the opposite chirality sector. We then calculate the first 100-200 eigenvalues of this projected overlap Dirac operator and extract the eigenvalues of D_{ov} from them. We henceforth denote the imaginary part of the n -th eigenvalue as λ_n . We have also checked that the real part of the first $\mathcal{O}(200)$ overlap eigenvalues is about two orders of magnitude smaller and hence sub-dominant compared to their imaginary part. This allows us to directly relate our study to the continuum case where the Dirac operator has only imaginary eigenvalues.

T (MeV)	β	c_5	L_5	N_s	N_τ	N_{eigen}	N_{confs}
164	1.725	1.5	16	32	8	100	95
177	1.771	1.0	16	32	8	100	93
195	1.829	0.9	16	32	8	100	108
270	2.130	0.5	24	32	8	150	122
314	2.250	0.5	12	32	8	200	111
339	2.310	0.5	12	32	8	200	92

Tab. I. Number of gauge configurations at different temperatures, $\beta = 6/g^2$ and lattice size used in this work. The table also lists the number of overlap Dirac eigenvalues calculated per gauge configuration, along with the values of the Möbius parameter c_5 and L_5 used in the generation of gauge ensembles at each temperature.

We have also calculated the correlation between real part of the renormalized Polyakov loop values with these first $\mathcal{O}(100)$ Dirac eigenstates. We performed our calculation using the gradient flow renormalization scheme using the Wilson gauge action [65]. The flow equation is solved using the fourth-order Runge-Kutta scheme with a step size of 0.01 up to a flow time t which should ideally be determined from the criterion $a \ll \sqrt{8t} \ll 1/T$. In order to ensure that this criterion is satisfied for all temperatures we have studied, the flow time in physical units was chosen to be $\sqrt{8t} = 0.44$ fm for $T \leq 195$ MeV and $\sqrt{8t} = 0.25$ fm for higher temperatures $T > 200$ MeV. We applied a constant shift in free energy to match with the earlier continuum extrapolated results from Ref. [66] at the highest temperature in order to fix the scale. This same shift in the free energy values for two lower temperatures 270 and 314 MeV also gave us an estimate of the renormalized Polyakov loop which is in good agreement with the continuum results mentioned in Ref. [66].

V. RESULTS

A. Level spacing ratios near the chiral crossover transition

We first calculate the spacings between the neighboring eigenvalues of the Dirac operator denoted as $s_n = \lambda_{n+1} - \lambda_n$. Instead of calculating the level spacing distribution, we study the normalized ratios of the consecutive level spacings defined as $\tilde{r}_n = \min(r_n, 1/r_n)$, where $r_n = s_{n+1}/s_n$. Such a construction eliminates the local dependence of spacing distributions on the eigenvalue level density [67]. Hence \tilde{r}_n is insensitive to systematic errors that arise while performing an unfolding of the spacing distribution, due to limited statistics and in small volumes. We have previously advocated its use for the first time to study localization properties of the eigenstates of the QCD Dirac operator [41]. Our results for $\langle \tilde{r} \rangle$ in bins of λ/T obtained after averaging over gauge configurations at $T \gtrsim T_{pc}$ are summarized in Fig. 1.

We first focus on $T = 164$ MeV which is just above the chiral pseudo-critical temperature. We observe that the $\langle \tilde{r} \rangle$ for eigenmodes in the lowest bin is in-between the values known for an uncorrelated and a Gaussian Unitary ensemble. We label them as *intermediate* eigenmodes. For all other bins, the average value of $\langle \tilde{r} \rangle = 0.602$ [41] is consistent with expectations from a GUE [68]. This categorization of Dirac eigenmodes into *intermediate* and bulk can be easily done from Fig.1 for other temperatures as well. At $T = 164$, 177 and 195 MeV, all eigenmodes which are below $\lambda/T = 0.12$, 0.33 and 0.6 respectively are designated as *intermediate* eigenmodes, whereas the ones above these values are identified as bulk eigenmodes. Note that at these temperatures, the singlet $U_A(1)$ subgroup of chiral symmetry remains significantly broken [28] instead only a remnant Z_2 subgroup is left intact.

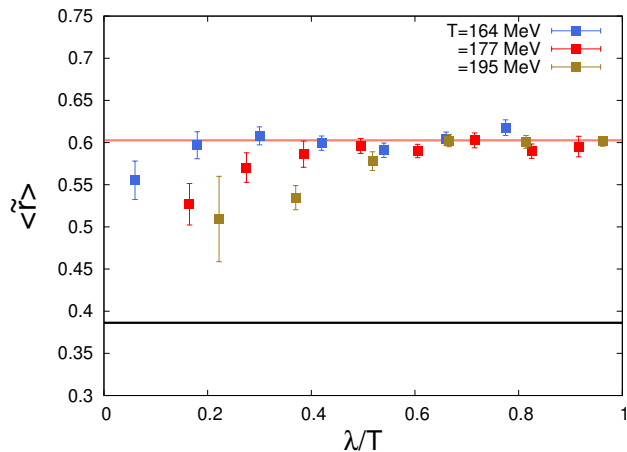


Fig. 1. The variation of $\langle \tilde{r} \rangle$ in bins of the Dirac eigenvalues λ/T in the temperature range where the non-singlet part of chiral symmetry is *effectively* restored but not its $U_A(1)$ subgroup. The orange and black solid lines represent the expected $\langle \tilde{r} \rangle$ for the eigenvalues with GUE and Poisson level statistics respectively.

Based on this information, we provide an interpretation for $\langle \tilde{r} \rangle$ of the *intermediate* eigenmodes in terms of universal properties of random matrices. We refer to a recent work on understanding universal level spacing ratios in random matrices comprising of several independent blocks of known Wigner surmises [69]. Following their construction, we model the average spacing ratio for these *intermediate* eigenvalues as a weighted sum denoted as $\langle \tilde{r} \rangle = w\langle \tilde{r} \rangle_1 + (1-w)\langle \tilde{r} \rangle_2$, where $\langle \tilde{r} \rangle_{1,2}$ are the average spacing ratios from a single GUE block and two GUE blocks respectively. Here, a single GUE block represents the contribution of bulk modes only, whereas a random matrix construction with two GUE blocks represents the scenario when the infrared eigenmodes that contribute to the chiral condensate and $U_A(1)$ breaking have admixture with the bulk eigenmodes. We remind here that the bulk eigenmodes survive even at temperatures when different subgroups of chiral symmetry are *effectively* restored. Using the values of $\langle \tilde{r} \rangle = 0.55$ for the *intermediate* eigenmodes at $T = 164$ MeV and $\langle \tilde{r} \rangle_1 = 0.602$ and $\langle \tilde{r} \rangle_2 = 0.3992$ from Ref. [69], we obtain the relative weight of the bulk eigenmodes to be $w = 0.74$. In contrast, the value for $\langle \tilde{r} \rangle$ for the lowest bin at $T = 149$ MeV [41] is consistent with one single GUE block because the $SU_A(2)$ and $U_A(1)$ subgroups of the chiral symmetry are explicitly broken and there are no remnant unbroken symmetries that can support the block-like decomposition.

B. Level spacing ratios in the region $T_{pc} < T < T_{U(1)}$

We would now like to address the question of what happens to the level spacing ratios of the *intermediate* eigenmodes in the temperature regime when the $U_A(1)$

subgroup of chiral symmetry is broken whereas the non-singlet subgroup is *effectively* restored. In this regime, the infrared eigenfunctions exhibit very interesting structural properties. We have earlier shown that at $T \sim 181$ MeV the *intermediate* eigenmodes have fractal-like features and calculated their fractal dimension D_f [41]. It was observed that the median value of $D_f \sim 2.5$ which can be understood from the fact that these eigenmodes carry information of the remnant $O(4)$ symmetry due to the *effective* restoration of the non-singlet $SU_A(2)$ subgroup of the chiral symmetry.

The $U_A(1)$ subgroup should also get *effectively* restored at a certain temperature $T_{U(1)}$, where the density of the smallest eigenvalues of the Dirac operator can be explained as arising due to a gauge background consisting of a dilute gas of instantons [28]. In such a case, these eigenvalues should follow level spacing distribution corresponding to an uncorrelated ensemble [70]. However as long as $U_A(1)$ is not *effectively* restored, the infrared Dirac eigenmodes will have mixing with the remnant tail end of the bulk eigenspectrum, resulting in intermediate level statistics. This is already evident in Fig. 1 where the average value $\langle \tilde{r} \rangle$ of the eigenmodes in the deep infrared bin is decreasing as a function of increasing temperature in the range $1.1 < T/T_{pc} < 1.2$. At these temperatures when the $U_A(1)$ is not yet *effectively* restored, we can model the lowest eigenvalues of the Dirac operator arising out of a matrix with a 2-block structure, one of them representing a matrix belonging to a GUE and the other to an uncorrelated ensemble. We have calculated the level spacing ratios in a 2-block system numerically and compared them with our lattice data, the details of which are discussed in Section V D.

C. Level spacing ratios in the region $T > T_{U(1)}$

At even higher temperatures $T > T_{U(1)}$, we expect that Dirac eigenvalues arising due to a gauge background consisting of a dilute gas of instantons will accumulate in the deep infrared part of the eigenvalue spectrum [29, 46], thus separating from the bulk through a gap. We observe this gap opening up in the eigenvalue spectrum as the temperatures are increased beyond 195 MeV. Note that the values of $\langle \tilde{r} \rangle$ in the lowest bin at $\lambda/T = 0.71, 0.80, 0.85$ for temperatures $T = 270, 314, 339$ MeV respectively, have a large signal-to-noise ratio related to rare occurrences of such eigenvalues, hence not shown explicitly in Fig. 2. We characterize all eigenmodes for which $\lambda/T < 1.0, 1.1$ and 1.2 at temperatures $T = 270, 314$ and 339 MeV respectively as *intermediate* eigenmodes since their $\langle \tilde{r} \rangle$ values are intermediate between a GUE and an uncorrelated matrix ensemble. Eigenvalues beyond these constitute the bulk eigenspectrum.

Extending the block-like construction discussed in the previous subsection and in section V D, one can interpret the $\langle \tilde{r} \rangle$ values in the bins just above the gap as arising due

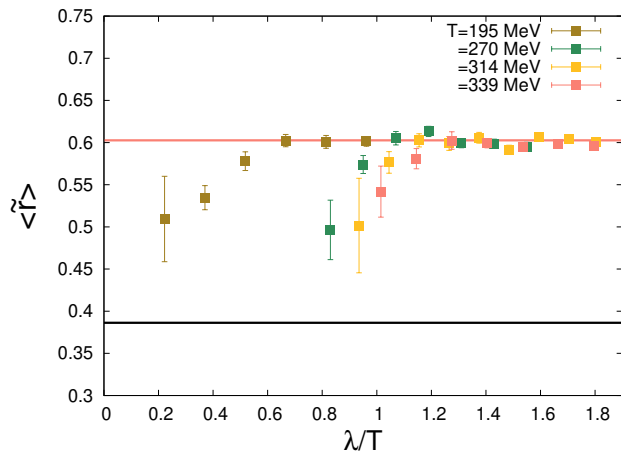


Fig. 2. The variation of $\langle \tilde{r} \rangle$ in small bins in λ/T at high temperatures $T \gtrsim 270$ MeV when the $U_A(1)$ is effectively restored, compared to the data at 195 MeV. The orange and black solid lines represent the expected $\langle \tilde{r} \rangle$ for the eigenvalues with GUE and Poisson level statistics respectively.

to mixing between the chaotic and localized regions of the bulk eigenspectrum. However, since the bulk spectrum is overwhelmingly chaotic with only a few localized eigenmodes in its tail, the $\langle \tilde{r} \rangle$ within the first few bins immediately approaches its GUE value as the temperature is increased. This is evidently different from the trend visible in the $\langle \tilde{r} \rangle$ data at $T = 195$ MeV, which is shown again in Fig. 2 for the sake of comparison. At this temperature, the gap is negligibly small, implying a larger fraction of the near-zero eigenmodes contributing to the $\langle \tilde{r} \rangle$, unlike the scenario at $T = 270$ MeV. Anderson-like localization phenomenon for the Dirac spectrum [31, 51, 71] has been studied in the same temperature regime discussed in this section. We provide a more detailed interpretation of our data in section V E and discuss how well these can be compared to a 3D Anderson model near the mobility edge [14, 72].

D. Interpreting the appearance of Dirac eigenvalues with intermediate level statistics

In this section, we outline how the normalized level ratios $P(\tilde{r})$, for eigenvalues appearing in the infrared part of the QCD Dirac spectrum, can give us important physical insights about their localization properties. Before we proceed, we summarize our lattice results for $P(\tilde{r})$ in the different regions of Dirac spectrum labeled as *intermediate* and *bulk*, as a function of temperature, in the left and right panels of Fig. 3 respectively. The $P(\tilde{r})$ for bulk eigenmodes for all the temperatures $T > T_{pc}$ are in excellent agreement with the prediction from random matrices belonging to GUE, as expected. The distribution $P(\tilde{r})$ for the *intermediate* eigenvalues is clearly different both from the expectations of uncorrelated eigenvalues as well as from a GUE. The questions we would like to address

are, firstly, what is the physical origin of these *intermediate* level ratios and how to replicate this in terms of a simple model of random matrices in terms of an admixture with uncorrelated eigenvalues. The amount of this admixture, in general, should be a function of temperature. An earlier study with the staggered Dirac spectrum in the continuum limit also observed distinctly different properties of the density of these so-called *intermediate* eigenvalues that proliferate when $SU_A(2)$ is effectively restored when compared with the most infrared eigen-density in the chiral symmetry broken phase [37].

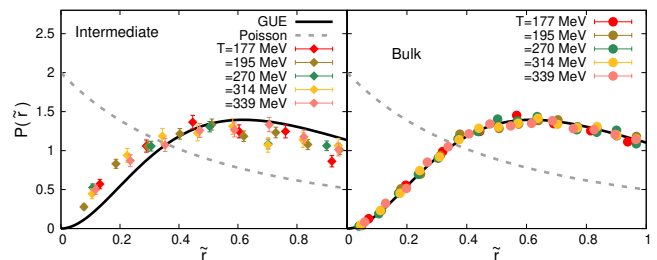


Fig. 3. Probability distribution of \tilde{r} for the *intermediate* (left) and bulk (right) eigenvalues at different temperatures compared with its values for random matrices belonging to GUE (solid line) and for uncorrelated eigenvalues following Poissonian level statistics (dotted line) respectively.

We follow three different approaches to model the distribution of \tilde{r} for the *intermediate* eigenvalues in the same spirit as, but by extending concepts from the random matrix theory. We construct our models starting with a random matrix belonging to GUE with 0.3 million eigenvalues. The probability distribution $P(\tilde{r})$ for the level ratios should follow the GUE prediction, which is confirmed and shown in Fig. 4 as a black solid line. As our first model, we construct a sufficiently small block of eigenvalues drawn from a uniform random distribution with a spacing distribution akin to uncorrelated eigenvalues following Poisson statistics whose size is 3% and 15% of the GUE block respectively. The eigenvalues of this block are chosen such that these lie within the range of the eigenvalues present in the GUE block except at the edges of this range, in order to allow for a complete mixture of the uncorrelated and GUE eigenvalues without any leakage. This is also done to mimic the QCD Dirac spectrum as closely as possible, where we do not observe any localized uncorrelated eigenvalues. Whenever a new eigenvalue is inserted between existing eigenvalues of the GUE block, three new normalized level ratios arise as a result, denoted as $\tilde{r}_{n_1}, \tilde{r}_{n_2}, \tilde{r}_{n_3}$. In order to be more explicit, let us assume that a new eigenvalue $\lambda_{n'}$ is inserted between the existing eigenvalues λ_n and λ_{n+1} of the GUE block such that the spectrum of the new mixed ensemble is denoted by $\lambda_0, \lambda_1, \dots, \lambda_{n-1}, \lambda_n, \lambda_{n'}, \lambda_{n+1}, \lambda_{n+2}, \dots, \lambda_{N-1}$. Here λ_i , where $i = 0, \dots, N-1$ are eigenvalues of our original GUE-block of size N . The three new level ratios that arise as a result are $r_{n_1} = \frac{\lambda_{n'} - \lambda_n}{\lambda_n - \lambda_{n-1}}$, $r_{n_2} = \frac{\lambda_{n+1} - \lambda_{n'}}{\lambda_{n+1} - \lambda_n}$

and $r_{n_3} = \frac{\lambda_{n+2} - \lambda_{n+1}}{\lambda_{n+1} - \lambda_n}$, which are normalized to give us $\tilde{r}_{n_i} = \min\left(r_{n_i}, \frac{1}{r_{n_i}}\right)$, $i = 1, 2, 3$. The new eigenvalues are accepted only if all three locally induced \tilde{r} are compatible with the target distribution, i.e. $P_{\text{GUE}}(\tilde{r})$, implemented through an independent accept-reject criterion. The acceptance probability of this newly selected eigenvalue is set to be $\prod_{i=1}^3 \frac{P_{\text{GUE}}(\tilde{r}_{n_i})}{P_{\text{GUE}}^{\text{max}}}$, where $P_{\text{GUE}}(\tilde{r})$ is the probability distribution of normalized ratios \tilde{r} for matrices belonging to GUE whereas $P_{\text{GUE}}^{\text{max}}$ is the maximum value possible for the distribution $P_{\text{GUE}}(\tilde{r})$.

Although the probability with which each new eigenvalue is accepted is the same as that of a GUE, for a sufficiently small block size of these newly chosen eigenvalues, it is obvious that the level repulsion between them is consistent with a Poisson distribution, as a priori no correlations exist between them. The probability distribution $P(\tilde{r})$ for the eigenvalues within this new block with block sizes 3% and 15% of the GUE-block respectively are also shown in Fig. 4. From the plot it is clearly evident that for a smaller block which is 3% of the original GUE-block, the $P(\tilde{r})$ agrees well with that known for a Poisson distribution. In the same figure, we have also shown $P(\tilde{r})$ for the full spectrum where existing eigenvalues from a GUE-block have an admixture of 3% and 15% of its size from the uncorrelated block, labeled as *mixed*. From Fig. 4, it is evident that this model cannot explain the $P(\tilde{r})$ for the *intermediate* Dirac eigenmodes shown in Fig. 3 for smaller values of \tilde{r} .

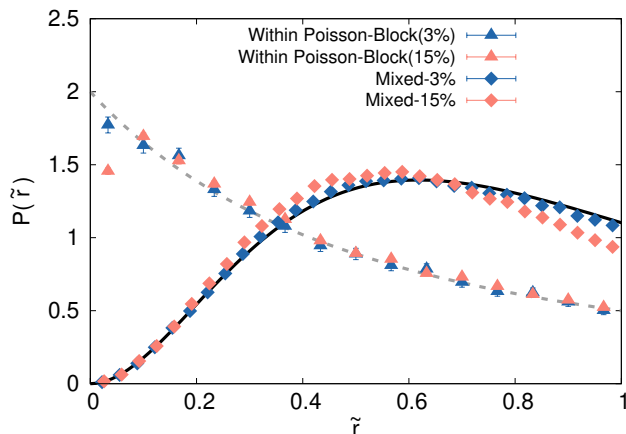


Fig. 4. Probability distribution of the normalized level ratios $P(\tilde{r})$ for our first matrix model (see the text for the details). The $P(\tilde{r})$ for the newly added uncorrelated block, and the entire mixed matrix are shown as triangles and diamonds respectively denoting 3% (blue) and 15% (orange) admixture. The $P(\tilde{r})$ for eigenvalues belonging to uncorrelated and GUE matrices are shown as dashed and solid lines respectively.

Our second model is designed in a manner similar to the first one but in this case the randomly chosen new eigenvalues are accepted within the existing GUE-block with a probability $\prod_{i=1}^3 \frac{P_{\text{P}}(\tilde{r}_{n_i})}{P_{\text{P}}^{\text{max}}}$. Here $P_{\text{P}}(\tilde{r})$ is the probability distribution of normalized level ratios \tilde{r} for un-

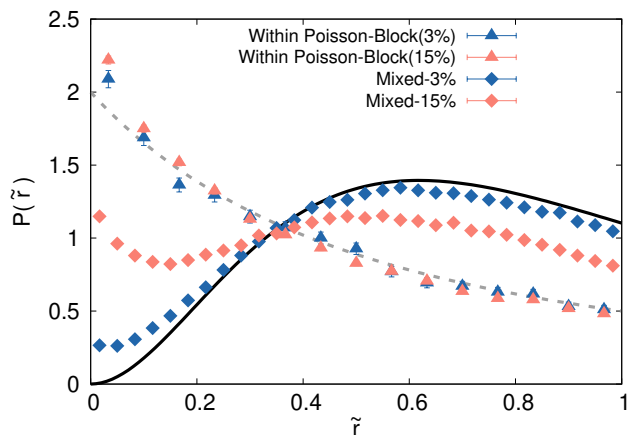


Fig. 5. Probability distribution of the normalized level ratios $P(\tilde{r})$ for our second matrix model (see the text for the details). The $P(\tilde{r})$ for the newly added uncorrelated block, and the entire *mixed* matrix are shown as triangles and diamonds respectively denoting 3% (blue) and 15% (orange) admixture. The $P(\tilde{r})$ for eigenvalues belonging to uncorrelated and GUE matrices are shown as dashed and solid lines respectively.

correlated eigenvalues following Poisson level statistics whereas $P_{\text{P}}^{\text{max}}$ is the maximum possible value for the distribution $P_{\text{P}}(\tilde{r})$. In this approach, eigenvalues that are closely spaced will be more favored. We show the results of our calculation of $P(\tilde{r})$ in Fig. 5, when the newly added eigenvalue blocks are of sizes which are 3% and 15% respectively of the original GUE block. The $P(\tilde{r})$ of the newly added eigenvalue block is close to the value for uncorrelated eigenvalues, as expected. The $P(\tilde{r})$ of the entire matrix consisting of GUE and Poisson blocks is labeled as *mixed* and is also shown in the same figure. For smaller values of \tilde{r} , the $P(\tilde{r})$ is intermediate between the values expected from Poisson and GUE level statistics respectively, which is quite different from the trend observed for *intermediate* eigenvalues of the QCD Dirac spectrum at all temperatures. This motivates us to formulate a third approach.

Our third matrix model will focus on improving the modeling of $P(\tilde{r})$ to more closely mimic the lattice data at smaller values of \tilde{r} . Our lattice data for *intermediate* eigenvalues shows some enhancement of $P(\tilde{r})$ compared to its magnitude in GUE for moderately small values of \tilde{r} , but the probabilities for the existence of eigenvalues with negligibly small spacing ratio $\tilde{r} \rightarrow 0$ are heavily disfavored. We model this fact in our random matrix construction by accepting newly generated eigenvalues with a probability $\prod_{i=1}^3 P_{\text{mix}}(\tilde{r}_{n_i})$, where $P_{\text{mix}}(\tilde{r}) \in \left\{ \frac{P_{\text{GUE}}(\tilde{r})}{P_{\text{GUE}}^{\text{max}}}, \frac{P_{\text{P}}(\tilde{r})}{P_{\text{P}}^{\text{max}}} \right\}$. Which of the two elements in this set decides the probability of accepting an eigenvalue depends on the values of $\tilde{r}_{n_1}, \tilde{r}_{n_2}, \tilde{r}_{n_3}$ and a threshold value of \tilde{r}_{max} chosen in our study to be $\tilde{r}_{\text{max}} = 0.05$. If the values of $\tilde{r}_{n_1}, \tilde{r}_{n_2}, \tilde{r}_{n_3} < 0.05$ then the $P_{\text{mix}}(\tilde{r}_{n_i}) = P_{\text{GUE}}(\tilde{r}_{n_i})$ else $P_{\text{mix}}(\tilde{r}_{n_i}) = P_{\text{P}}(\tilde{r}_{n_i})$. This selection cri-

terion thus explicitly avoids selecting new eigenvalues which will lead to the proliferation of smaller values of \tilde{r} . The probability distributions $P(\tilde{r})$ for the newly added eigenvalues constituting a block of size 3% and 15% of the existing GUE block respectively for this *mixed* model are shown in Fig. 6. For the smaller block size of the newly accepted eigenvalues, which comprises 3% of the original GUE-block, the repulsion among the closely spaced eigenvalues is similar to expectations in a Poisson ensemble. In the same figure, we have also compiled our results for $P(\tilde{r})$ of the entire matrix consisting of both GUE and uncorrelated blocks which we consistently label as *mixed*. The $P(\tilde{r})$ for the eigenvalues chosen in this hybrid approach with a 3-15% admixture can explain our lattice data for the normalized level ratios of *intermediate* Dirac eigenvalues for a wide range of temperatures between 177-339 MeV. This is shown in Fig. 7 where the band represents the prediction from our model 3 with an admixture in the range ~ 3 -15%. Note, however, that the amount of admixture might vary within each small bin in λ/T and its precise determination in the far infrared part of the spectrum will require further improvement in statistics.

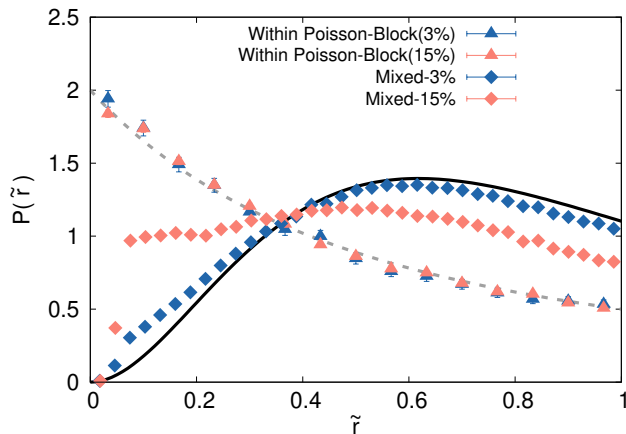


Fig. 6. Probability distribution of the normalized level ratios $P(\tilde{r})$ for our third matrix model (see the text for the details). The $P(\tilde{r})$ for the newly added uncorrelated block, and the entire mixed matrix are shown as triangles and diamonds, respectively denoting 3% (blue) and 15% (orange) admixture. The $P(\tilde{r})$ for eigenvalues belonging to uncorrelated and GUE matrices are shown as dashed and solid lines respectively.

We will now elaborate on a physical understanding of these models, i.e. why our model 3 can realistically describe the universal level spacing ratios for the *intermediate* Dirac eigenvalues in different temperature regimes. Dyson provided an intuitive understanding [73] of the level spacing distribution of eigenvalues ϵ_i of a $N \times N$ random matrix by modeling them as fictitious Brownian point particles moving in one dimension at finite temperature, whose inverse is the Dyson index β . The potential that describes the Brownian motion of the eigenvalues consists of a confining as well as a repulsive part given

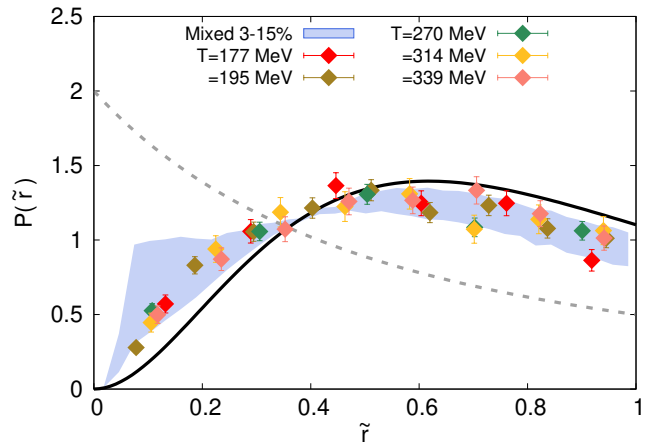


Fig. 7. The probability distribution of \tilde{r} at different temperatures for *intermediate* Dirac eigenmodes compared to the values obtained in our matrix model 3 shown as a blue band. The band represents values of $P(\tilde{r})$ corresponding to 3-15% mixing described within our matrix model 3. The $P(\tilde{r})$ for eigenvalues belonging to uncorrelated and GUE matrices are shown as dashed and solid lines respectively.

by $V(\{\epsilon_i\}) = \sum_{i=1}^N \epsilon_i^2 - \sum_{i < j} \log |\epsilon_i - \epsilon_j|$, where i, j label the eigenvalues. Performing a Monte-Carlo simulation of this system of $N = 1000$ Brownian particles, the distribution of the normalized level spacing ratios of a random matrix belonging to GUE can be reproduced.

Now, in order to understand the origin of *intermediate* level statistics in terms of Dyson's construction, we replace the harmonic oscillator potential with another choice which causes a weaker confinement [74, 75]. The choice of different weak confining potentials was originally motivated in order to construct different classes of random matrix ensembles that have multi-fractal eigenfunctions and to understand what characteristic signatures of such multifractality are inherent in the spacing distribution [75]. For one such choice of a confining potential, $V(\{\epsilon_i\}) = A \sum_i \ln^2 |\epsilon_i|$, we obtain a normalized level spacing ratio distribution which can very well explain our lattice data for the *intermediate* Dirac eigenvalues, shown in Fig. 8. Though in our calculation we have chosen $A = 0.2$, we have verified that level spacing ratio distributions are independent of the strength of potential denoted by A , by varying it sufficiently such that $A \in [0, 10]$. Another different choice of a weaker confining potential [74], $V(\{\epsilon_i\}) = A \sum_i |\epsilon_i|^\alpha$ can explain our lattice data consistently as well.

We summarize our attempts to understand the onset of the *intermediate* region in the Dirac eigenspectrum starting from predominantly chaotic eigenvalues in the bulk and quantify the probability distribution of their normalized level ratios. By varying the fractional admixture of uncorrelated eigenvalues introduced within a large GUE matrix block according to a very specific criterion which is discussed above in model 3, the deviation of $\langle \tilde{r} \rangle$ from its GUE prediction can be very well understood for

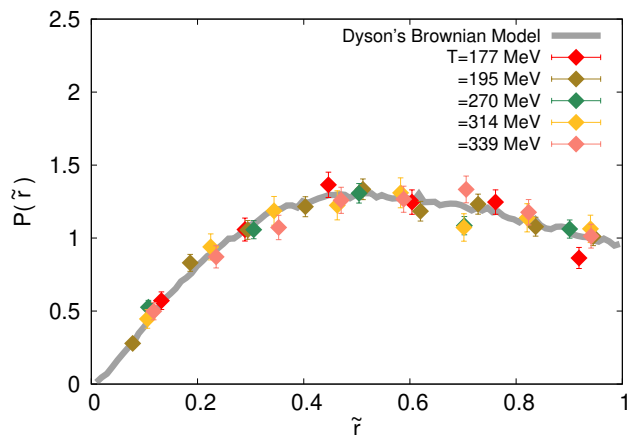


Fig. 8. The probability distribution for \tilde{r} obtained using Dyson's Brownian model for eigenvalues $\{\epsilon_i\}$ moving in presence of a weak confining potential along with a log-repulsion between them, shown as a solid line. The probability distributions of \tilde{r} for the Dirac eigenvalues with *intermediate* level statistics, at different temperatures, are also shown (as points) for comparison.

the infrared Dirac eigenvalues. The matrix model has a nice interpretation in terms of Dyson's construction of a Brownian model of eigenvalues as well. Our matrix model 3 is very general and versatile, which can describe the probability distribution $P(\tilde{r})$ for *intermediate* eigenvalues appearing as a result of different physical mechanisms at work at different temperatures. This is evident in the trend visible in the data for $\langle \tilde{r} \rangle$. Compared to $T = 195$ MeV, one observes that the values of $\langle \tilde{r} \rangle$ at $T = 314$ MeV deviate from the bulk more dramatically within the span of a few bins while moving towards the infrared. Typically, at temperatures $T < T_{U(1)}$, when the (anomalous) singlet subgroup of chiral symmetry is not *effectively* restored, the amount of admixture with uncorrelated eigenvalues spans over a larger range in λ , gradually increasing as one moves towards the infrared bins. At $T \simeq T_{U(1)}$, intermediate values of $\langle \tilde{r} \rangle$ are found only in the lowest few eigenvalue bins and tend to be even closer to an uncorrelated distribution. This might be due to an efficient separation of the near-zero and bulk eigenvalues [37] in this temperature regime, leading to an *effective* restoration of $U_A(1)$.

Similar analysis for the distribution of level ratios has been performed on a mixed ensemble of Poisson-GOE matrices in Ref. [76] by generalizing the techniques formulated in Ref. [69] for understanding mixing between eigenvalues of matrices belonging to different symmetry classes [77]. These works [69, 76] derive the joint distribution of consecutive nearest-neighbor level spacings of a compound spectrum constructed out of spectra with different distributions. However for a Poisson-GUE system, there is no analytic solution of the normalized level spacing ratios in this approach, which have to be determined numerically. Our numerical approach is thus another way

to explain a mixed ensemble of matrices belonging to two different symmetry categories. We also note that modeling a mixed level-spacing distribution has also been discussed in the literature heuristically in terms of a best fit function with few parameters [78]. A microscopic model consisting of a two-dimensional matrix mimicking a Poisson process weakly coupled with a random matrix belonging to different Wigner surmise [79–81] has also been shown to fit a mixed distribution in terms of a single parameter that denotes the strength of the coupling.

E. Understanding the origin of disorder and (de)localization in QCD Dirac eigenstates

Having interpreted the Dirac eigenmodes with intermediate level statistics as arising due to an admixture between eigenvalues with universal level spacing fluctuations of GUE and Poisson ensemble, we would now like to understand the microscopic origin of such a mixing.

We recall that in the Euclidean formalism, the partition function of QCD can be realized as a path integral with fermion fields satisfying anti-periodic boundary conditions along the compact imaginary time of extent $1/T$. As a result, the lowest eigenvalue of the Euclidean lattice Dirac operator for non-interacting quarks is $\sin(\pi/N_\tau)$. Turning on gauge interactions, the temporal part of the Dirac operator can be diagonalized in the limit of weak coupling in terms of diagonal elements at each lattice site which is the lowest Matsubara mode shifted by the local Polyakov loop values [81]. A random matrix model of these local Matsubara modes with nearest-neighbor interactions closely resembles the tight-binding Anderson model [81]. At high temperatures, the fluctuations of the Polyakov loop below its mean become rarer and occur at random spatial locations [31, 82, 83], justifying its resemblance to a random disordered potential. However, the validity of these assumptions needs to be revisited for temperatures $T_{pc} < T < T_{U(1)}$. We will address this point in this section.

In the regime $T \gtrsim T_{pc}$, the regions with strong fluctuations in the local values of Polyakov loop are typically (anti)correlated with the probability density for the occurrence of instanton-dyons [84] which form a semiclassical gas [85, 86]. Hence, the origin of disorder at temperatures T_{pc} is largely driven by fluctuations about the topological vacuum in QCD. In this regime, the temperature dependence of topological susceptibility is different from that of a dilute instanton gas [27]. This is the same region where $U_A(1)$ remains badly broken precisely because of these non-trivial topological fluctuations. When temperatures are $T \gtrsim 1.5 T_{pc}$, the holonomy becomes trivial and the sites with discernible random fluctuations of the Polyakov loop values are no longer correlated with the fluctuations of the topological vacuum in QCD. Incidentally, this is the regime when $U_A(1)$ is believed to be *effectively* restored and randomness in the fluctuations of local Polyakov loop should be solely driven by the inher-

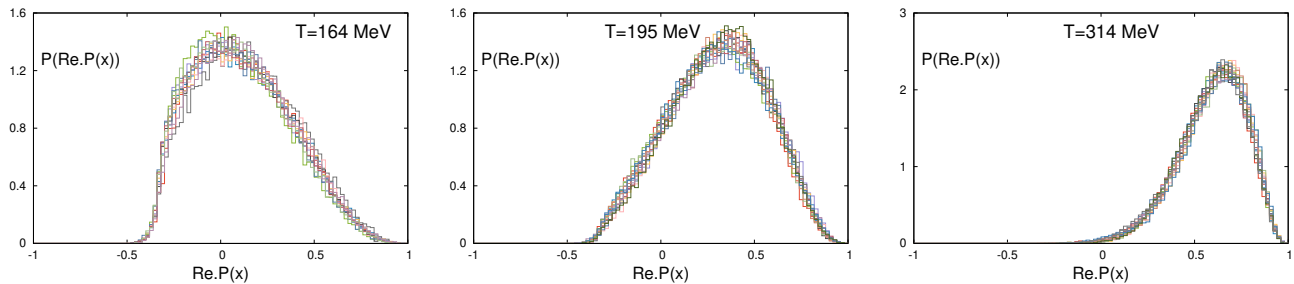


Fig. 9. Probability distribution of the $\text{Re}.P(\mathbf{x})$ for statistically independent gauge configurations, calculated after performing Wilson flow renormalization at three different temperatures above the chiral crossover transition. The three panels from left to right correspond to different temperatures $T = 164, 195$ and 314 MeV.

ent chaotic nature of color interactions [87, 88].

We also review the literature to clarify some important points that are not often discussed in the study of Anderson localization in QCD. Firstly, since the gauge field configurations represent a strongly interacting many-body system at $T_{pc} < T < T_{U(1)}$, it is not clear a priori whether the noise inherent in it can be considered as random, as required in the Anderson model. The generalization of Anderson localization in interacting systems, known as many-body localization (MBL), has been discussed as a finite temperature phase transition [89] and is currently under intensive review [8, 90]. The characteristic signatures of MBL have been shown to be manifest in many single particle observables as well [91]. It is important to note that the disorder inherent in the gauge fields in QCD as a function of temperature is not quenched (static) but dynamically generated due to self-interactions similar to a scenario discussed in the context of interacting lattice spin models [92].

Secondly, we would like to remind here that when we calculate eigenvectors of the Dirac operator in presence of a noisy gauge background, we are solving for relativistic single particle states. This is different from a conventional Anderson model which discusses non-relativistic electrons in presence of a quenched random disorder. Anderson transition has been studied in three-dimensional non-interacting Dirac semimetals in presence of quenched disorder [93]. It was reported that such systems have three distinct ground states, i.e., an incompressible semimetal, a compressible diffusive metal, and an insulator, which is in contrast to a conventional Anderson model that describes a transition between only the latter two phases. In presence of a small amount of disorder, there is a quantum phase transition from a semimetal to a dirty metal phase, which, on increasing disorder strength by about six times, goes over to an insulating phase through the conventional Anderson semimetal-insulator transition. In our earlier study in quenched SU(3) gauge theory at $T \sim 600$ MeV, we did not observe any localized Dirac eigenstate in the deep infrared part of the spectrum [41], which characterizes an insulating phase. This absence of localized eigenmodes

may be attributed to the weakening of the disorder in the gauge fields. Hence, it is imperative that we make a more quantitative estimate of the amount of disorder inherent in the gauge fields in QCD, as a function of temperature.

For this purpose, we have calculated the renormalized Polyakov loop values at each spatial site of the lattice after performing gradient flow, details of which are mentioned in Sec. IV. We show the probability distribution of renormalized values of the real part of the Polyakov loop at each site \mathbf{x} , denoted as $\text{Re}.P(\mathbf{x})$ for a large set of gauge configurations, superposed together, and at different temperatures in Fig. 9. We observe that the width of these distributions is decreasing with increasing temperatures, demonstrating that gauge fields become smoother at higher temperatures. At higher temperatures $T = 314$ MeV, the large negative fluctuations in $\text{Re}.P(\mathbf{x})$ about its average value become rarer, resulting in a clear separation among these potential wells which are located at random sites. In contrast, close to the crossover transition at $T = 164$ MeV, the fluctuations in the renormalized values of the Polyakov loop are much more frequent and thus correlated. At the intermediate temperature $T = 195$ MeV, the confining wells still have a significant overlap with each other. This is also evident in the density plots of the local fluctuations of the Polyakov loop which are lower than its mean value at three different temperatures, shown in Fig. 10.

In order to quantify how well these deep negative fluctuations of the renormalized Polyakov loop $\text{Re}.P(\mathbf{x})$ about its mean are correlated with the Dirac eigenstates at each temperature, we calculate the quantity $C_n = \sum_{\mathbf{x}} |\Psi_n(\mathbf{x})|^2 [\text{Re}.P(\mathbf{x}) - \langle \text{Re}.P(\mathbf{x}) \rangle]$. Here the norm $|\Psi_n(\mathbf{x})|^2 = \sum_{\tau=0}^{N_\tau-1} |\psi_n(\mathbf{x}, \tau)|^2$ at each spatial site \mathbf{x} on the lattice is obtained by summing over the density of the n^{th} eigenstate of the overlap Dirac operator in four dimensions along the temporal direction τ . We calculate the net correlation $C(\lambda/T)$ by performing a binning of the C_n , calculated for each eigenstate labeled by n , in small bins in λ/T and performing an average over the gauge configurations for different temperatures, results of which are compiled in Fig. 11. It is evident from the figure that eigenvalues in the *intermediate* region of the

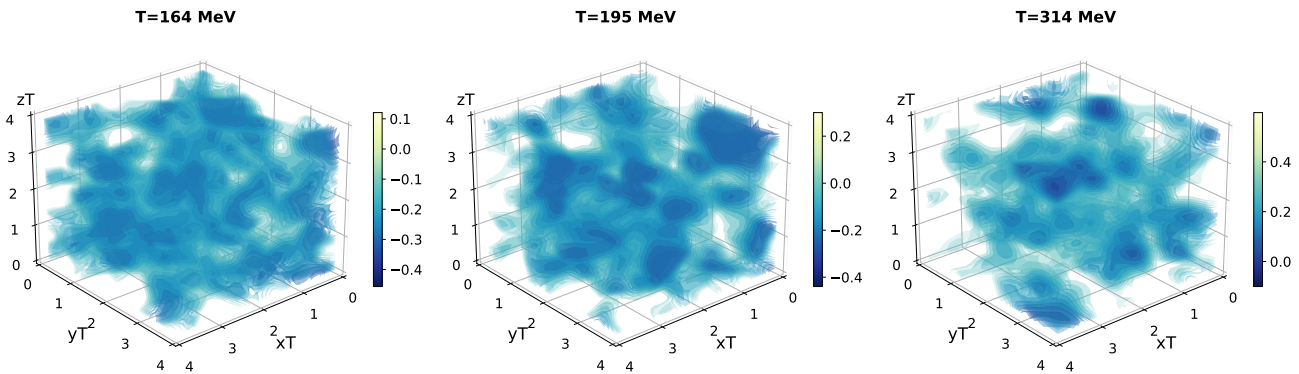


Fig. 10. Visual representation of the local fluctuations in the real part of the Polyakov loop $\text{Re}.P(\mathbf{x})$ which are below its mean value, obtained after performing Wilson flow renormalization on a typical gauge configuration. The lightest color in the palette represents its mean value in that particular configuration. The three panels from left to right correspond to different temperatures $T = 164, 195$ and 314 MeV.

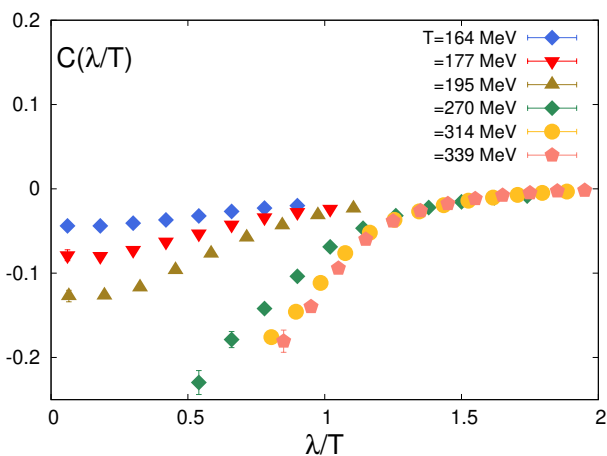


Fig. 11. The correlation $C(\lambda/T)$ between the local density of the Dirac eigenstate and the local fluctuation of $\text{Re}.P(\mathbf{x})$, evaluated in small bins of λ/T at different temperatures.

Dirac spectrum are more strongly correlated with the wells arising due to fluctuating renormalized Polyakov loop values as compared to the bulk eigenmodes. This demonstrates that indeed random local fluctuations in $\text{Re}.P(\mathbf{x})$ act as confining potentials for these low eigenmodes at high temperatures; nonetheless, it will be important to confirm this finding on a larger volume. The bulk eigenstates are delocalized chaotic states and hence do not feel these tiny local fluctuations.

At $T \leq 195$ MeV, the correlation between *intermediate* Dirac eigenstates with the local Polyakov loop fluctuations is weaker compared to temperatures $T > 250$ MeV. This is due to the fact that these well-like fluctuations at different lattice sites are no longer rare events at $T \leq 195$ MeV; on the contrary, they are strongly correlated, as also observed in Fig. 9. As a result, *intermediate* eigenstates are delocalized over several such locations. This is also evident from the spectral properties [40] and fractal-like feature [41] of these *intermediate* eigenstates

at $T < T_{U(1)}$ observed in previous works. In conclusion, the localization of the *intermediate* Dirac eigenstates in wells created due to fluctuations of $\text{Re}.P(\mathbf{x})$ is only apparent when $T > T_{U(1)}$.

F. Structural features of the Dirac eigenfunctions from Thouless conductance

Apart from the local correlations that are observed, e.g. in the spacing ratios, it is also important to identify global correlations that exist in the eigenspectrum. This will allow us to identify the physical origin of correlations that result in distinct structural changes in the eigenfunctions of the Dirac operator as a function of temperature.

One such quantity sensitive to global correlations is the Thouless conductance, which is measured in terms of the average shift in eigenvalues of the Hamiltonian of a quantum system due to a change in the boundary conditions along a spatial direction [59]. According to the Thouless criterion, one could then categorize eigenstates as extended or localized if the average shift is much larger than the average level spacing or vice versa. In our context, if the fermion fields ψ_i satisfy the boundary condition $\psi_i(x+L) = \psi_i(x)e^{i\eta}$ along any of the spatial directions of length L , this would modify the Dirac operator. As a result, its i -th eigenvalue should acquire a curvature K_i defined as $K_i = |\frac{\partial^2 \lambda_i}{\partial \eta^2}|$. The twist η should be infinitesimally small, i.e. $\eta \rightarrow 0$. We have chosen η such that the change in eigenvalues after applying the twist is larger than the numerical precision of $\sim 10^{-10}$ with which the eigenvalues are calculated. We have chosen $\eta = 0.005$ for our calculations. We have also verified that using $\eta = 0.01$ does not lead to any change in our results. We then compute the probability distribution of the curvature values, $P(K)$, separately for the *intermediate* and bulk eigenmodes. This is achieved by constructing appropriate bins for the normalized curvature values, $K_i \rightarrow K_i/\langle K \rangle$, where $\langle K \rangle$ denotes the average curvature

for the *intermediate* and bulk modes, respectively. After performing an ensemble average over available gauge configurations, the resulting distributions $P(K)$ for four different temperatures are shown in Fig. 12.

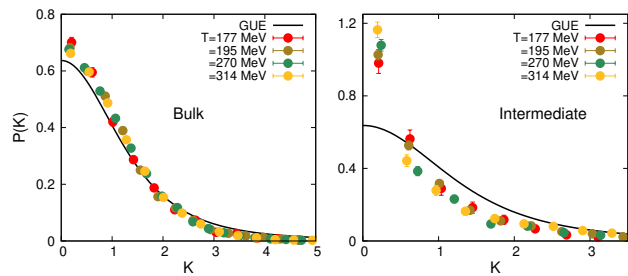


Fig. 12. The curvature distribution of the bulk (left) and *intermediate* (right) Dirac eigenmodes as a function of temperature. The black solid line represents the expected probability distribution for the curvature K for eigenvalues of random matrices belonging to a GUE.

Bulk eigenstates which are delocalized over the entire volume, should acquire larger curvature upon applying a twist compared to *intermediate* eigenstates whose inverse participation ratios do not scale inversely with volume. There can, however, be rare large fluctuations in the curvature distribution due to localized eigenstates that might be situated close to the boundaries of the lattice box. Our lattice data for the curvature distribution of the *intermediate* eigenmodes, shown in the right panel of Fig. 12, are consistent with these expectations. We have also compared the curvature distribution of bulk eigenmodes with the expectation from a GUE [94], given as $P(K) = \frac{2}{\pi} \frac{1}{(K^2+1)^2}$. As evident from Fig. 12, there is a fairly good agreement between $P(K)$ for bulk eigenmodes with the prediction from a GUE, for all temperatures we have studied.

We next calculate the Thouless conductance, defined as $g_{\text{Th}} = \frac{1}{\langle s \rangle} \langle K_i \rangle_{\eta \rightarrow 0}$ in terms of the curvature K_i acquired by the i -th eigenstate subject to an infinitesimally small twist η . Calculating averages for the curvatures $\langle K_i \rangle$ and level spacings $\langle s \rangle$ in small bins in λ/T at four different temperatures, we summarize our results for g_{Th} in Fig. 13. The g_{Th} is non-vanishing in the *intermediate* region, which implies that these eigenstates are not exponentially localized. Performing a fit to the data for bulk eigenvalues with an ansatz function that is linear in λ , we obtain a positive slope $dg_{\text{Th}}(\lambda/T)/d(\lambda/T)$ which has mild sensitivity to the change in temperature. The functional dependence of the Thouless conductance on λ/T in the bins containing *intermediate* eigenvalues is different compared to those with bulk eigenmodes. Thus g_{Th} allows us to unambiguously disentangle the bulk eigenvalues from the rest.

We show our results for g_{Th} as a function of temperature, only due to *intermediate* eigenmodes in Fig. 14. We have chosen only the lowest few *intermediate* eigenvalues, which are strongly correlated with the gauge field fluctuations, quantified in terms of $C(\lambda/T)$. It is clear that with

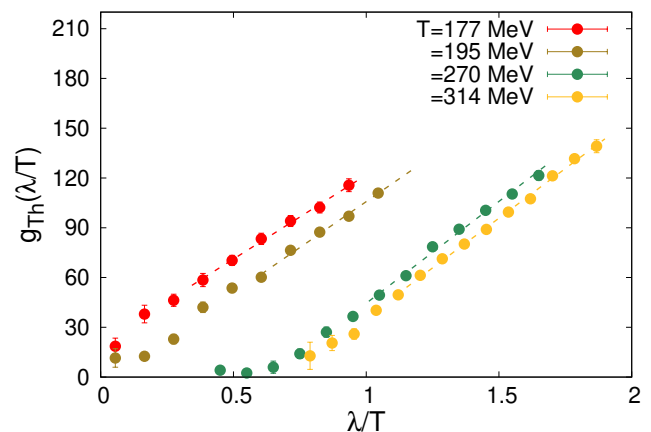


Fig. 13. The Thouless conductance for different eigenvalue bins calculated at temperatures $T = 177, 195, 270, 314$ MeV respectively. The dashed line represents a linear fit to the $g_{\text{Th}}(\lambda/T)$ for bulk eigenmodes.

increasing temperatures, these *intermediate* eigenmodes get more and more localized within the wells formed due to fluctuations in $\text{Re}P(\mathbf{x})$, leading to a reduction in the Thouless conductance. Value of g_{Th} drops very fast between 1.1 - $1.5 T_{pc}$, saturating at higher temperatures $T > T_{U(1)}$, albeit with large errors due to fewer eigenmodes in the lowest bins and possibly finite-volume effects. The observable g_{Th} can mimic as an *order parameter* for the *effective restoration* of $U_A(1)$ since the point of inflection of the curve that characterizes g_{Th} versus temperature could give us an estimate of $T_{U(1)}$. Noting that $U_A(1)$ is not an exact symmetry, one cannot construct an order parameter that conventionally characterizes a thermal phase transition within the Landau paradigm. We thus propose that the *effective restoration* $U_A(1)$ should be inferred from the change in the structural properties of the Dirac eigenstates, which can be quantified in terms of observables like g_{Th} .

VI. SUMMARY AND OUTLOOK

In this work, we have performed a detailed lattice study of the properties of infrared eigenstates of the massless Dirac operator on thermal gauge ensembles, in order to understand the high-temperature phase of a strongly correlated system described by QCD. We particularly focused on the question: how can we identify the *effective restoration* of the anomalous $U(1)$ subgroup of chiral symmetry using spectral and structural properties of the Dirac eigenstates and what are its physical consequences. We have performed our calculations with an extensive set of gauge configurations generated using Möbius domain wall fermion discretization, over a range of temperatures up to $\sim 2 T_{pc}$. Using normalized level spacing ratios of eigenvalues of massless 1-particle states realized using the overlap Dirac operator, we have unambiguously identified

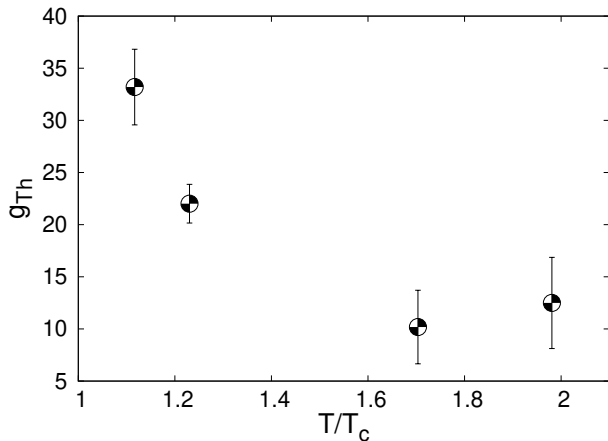


Fig. 14. Thouless conductance for the *intermediate* eigenmodes which have similar values of $C(\lambda/T)$, shown as a function of temperature.

those eigenmodes which have intermediate level statistics from the overwhelming majority of the bulk eigenstates. These bulk eigenstates have level repulsions consistent with random matrices belonging to a GUE. Though we have earlier provided an explanation for the existence of these *intermediate* eigenstates just above T_{pc} as arising due to the restoration of the non-singlet part of the almost exact chiral symmetry for QCD with two light quark flavors [41], however, we show here that their persistence at very high temperature has a different physical origin.

By studying the correlation of these *intermediate* eigenstates with fluctuations of the real values of the renormalized Polyakov loop about its mean, we could clearly show their distinct physical properties at high temperatures $T > 250$ MeV, where the axial U(1) symmetry is expected to be effectively restored, compared to $T < 200$ MeV, where it remains broken. In fact, the density plots for the real part of the renormalized Polyakov loop reveal that at $T > 250$ MeV, there are deep localized fluctuations at random sites of the lattice which are uncorrelated with each other, mimicking random disorder as discussed in the context of the Anderson model of electrons. We will study the finite volume effects more carefully in the future to understand whether these infrared eigenstates with intermediate level ratios describe the physics near the mobility edge in an Anderson-like transition. We also showed that fluctuations in the real

values of the renormalized Polyakov loop at different lattice sites are strongly correlated at $T < 200$ MeV, quite unlike the original proposal of a random disorder by Anderson. Our study hints at the fact that localization of the most infrared Dirac eigenstates will start to become more prominent when the axial U(1) subgroup of chiral symmetry is effectively restored.

We then provide an explanation for the existence of these Dirac eigenstates with intermediate level statistics within a matrix model. By introducing additional uncorrelated eigenvalues within a large random matrix belonging to a GUE with a very specific accept/reject criterion, we showed that normalized level ratios of this enlarged matrix can beautifully explain intermediate level ratios of the QCD Dirac eigenvalues shown in Fig. 7. We also discussed an intuitive understanding of such a matrix model construction in terms of a Brownian model describing the dynamics of the eigenvalues. Unlike the eigenvalues of a random matrix belonging to a GUE whose level separations arise due to its Brownian motion in a thermal bath with a weak log-repulsion and a strong confining harmonic potential, the intermediate eigen level ratios can be explained if the confining potential is weakened.

We also for the first time calculate the analogue of the Thouless conductance g_{Th} of the Dirac eigenstates which quantifies their structural rigidity when subject to a twist applied along one of the spatial boundaries of the lattice box. We use the curvature distribution and the g_{Th} to also independently distinguish between the *intermediate* eigenstates and the bulk. Calculating the g_{Th} only for the *intermediate* eigenstates that are strongly correlated with the local Polyakov loop fluctuations, we demonstrate its gradual decrease as a function of temperature. The point of inflection of this curve could give us an estimate of the temperature where $U_A(1)$ is *effectively* restored, and we will study this observable at larger volumes to firmly establish our claim in a future work.

VII. ACKNOWLEDGMENTS

We are grateful to Robin Kehr and Lorenz von Smekal for discussions on related topics during the course of this work. The authors acknowledge the use of High Performance Computing resources at the Institute of Mathematical Sciences. Our GPU code is in part based on some of the publicly available QUDA [95] and Grid Python Toolkit [96] libraries.

-
- [1] O. Bohigas, M. J. Giannoni, and C. Schmit, Phys. Rev. Lett. **52**, 1 (1984).
 [2] M. V. Berry and M. Tabor, Proceedings of the Royal Society of London. A. Mathematical and Physical Sciences **356**, 375 (1977).
 [3] J. M. Deutsch, Rept. Prog. Phys. **81**, 082001 (2018), arXiv:1805.01616 [quant-ph].

- [4] O. Bohigas, S. Tomsovic, and D. Ullmo, Phys. Rept. **223**, 43 (1993).
 [5] M. V. Berry and M. Robnik, Journal of Physics A: Mathematical and General **17**, 2413 (1984).
 [6] T. Prosen and M. Robnik, Journal of Physics A: Mathematical and General **27**, 8059 (1994).

- [7] S. H. Tekur, S. Kumar, and M. S. Santhanam, Phys. Rev. E **97**, 062212 (2018).
- [8] R. Nandkishore and D. A. Huse, Ann. Rev. Condensed Matter Phys. **6**, 15 (2015), arXiv:1404.0686 [cond-mat.stat-mech].
- [9] M. Serbyn and J. E. Moore, Phys. Rev. B **93**, 041424 (2016), arXiv:1508.07293 [cond-mat.dis-nn].
- [10] M. Amini, E. Cuevas, I. M. Khaymovich, and V. E. Kravtsov, New J. Phys. **17**, 122002 (2015).
- [11] S. Moudgalya and O. I. Motrunich, Phys. Rev. X **12**, 011050 (2022), arXiv:2108.10324 [cond-mat.stat-mech].
- [12] S. Moudgalya, B. A. Bernevig, and N. Regnault, Rept. Prog. Phys. **85**, 086501 (2022), arXiv:2109.00548 [cond-mat.str-el].
- [13] D. Adler, D. Wei, M. Will, K. Srakaew, S. Agrawal, P. Weckesser, R. Moessner, F. Pollmann, I. Bloch, and J. Zeiher, Nature **636**, 80 (2024), arXiv:2404.14896 [cond-mat.quant-gas].
- [14] B. I. Shklovskii, B. Shapiro, B. R. Sears, P. Lambrianides, and H. B. Shore, Phys. Rev. B **47**, 11487 (1993).
- [15] P. W. Anderson, Phys. Rev. **109**, 1492 (1958).
- [16] D. Das, L. Ebner, S. V. Kadam, I. Raychowdhury, A. Schäfer, and X. Yao, (2025), arXiv:2509.18269 [hep-th].
- [17] S. Sharma, PoS **CPOD2017**, 086 (2018).
- [18] M. P. Lombardo and A. Trunin, Int. J. Mod. Phys. A **35**, 2030010 (2020), arXiv:2005.06547 [hep-lat].
- [19] A. V. Smilga and J. Stern, Phys. Lett. B **318**, 531 (1993).
- [20] A. Bazavov *et al.* (HotQCD), Phys. Lett. B **795**, 15 (2019), arXiv:1812.08235 [hep-lat].
- [21] F. Burger, E.-M. Ilgenfritz, M. P. Lombardo, and A. Trunin, Phys. Rev. D **98**, 094501 (2018), arXiv:1805.06001 [hep-lat].
- [22] S. Borsanyi, Z. Fodor, J. N. Guenther, R. Kara, S. D. Katz, P. Parotto, A. Pasztor, C. Ratti, and K. K. Szabo, Phys. Rev. Lett. **125**, 052001 (2020), arXiv:2002.02821 [hep-lat].
- [23] J. J. M. Verbaarschot, Phys. Rev. Lett. **72**, 2531 (1994), arXiv:hep-th/9401059.
- [24] J. J. M. Verbaarschot and I. Zahed, Phys. Rev. Lett. **70**, 3852 (1993), arXiv:hep-th/9303012.
- [25] J. J. M. Verbaarschot, Nucl. Phys. B Proc. Suppl. **53**, 88 (1997), arXiv:hep-lat/9607086.
- [26] T. Kanazawa and M. Kieburg, J. Phys. A **51**, 345202 (2018), arXiv:1804.03985 [math-ph].
- [27] P. Petreczky, H.-P. Schadler, and S. Sharma, Phys. Lett. B **762**, 498 (2016), arXiv:1606.03145 [hep-lat].
- [28] R. V. Gavai, M. E. Jaensch, O. Kaczmarek, F. Karsch, M. Sarkar, R. Shanker, S. Sharma, S. Sharma, and T. Ueding, Phys. Rev. D **111**, 034507 (2025), arXiv:2411.10217 [hep-lat].
- [29] V. Dick, F. Karsch, E. Laermann, S. Mukherjee, and S. Sharma, Phys. Rev. D **91**, 094504 (2015), arXiv:1502.06190 [hep-lat].
- [30] S. Sharma, V. Dick, F. Karsch, E. Laermann, and S. Mukherjee, Nucl. Phys. A **956**, 793 (2016), arXiv:1602.02197 [hep-lat].
- [31] L. Holicki, E.-M. Ilgenfritz, and L. von Smekal, PoS **LATTICE2018**, 180 (2018), arXiv:1810.01130 [hep-lat].
- [32] A. Tomiya, G. Cossu, S. Aoki, H. Fukaya, S. Hashimoto, T. Kaneko, and J. Noaki, Phys. Rev. D **96**, 034509 (2017), [Addendum: Phys.Rev.D 96, 079902 (2017)], arXiv:1612.01908 [hep-lat].
- [33] S. Aoki, Y. Aoki, G. Cossu, H. Fukaya, S. Hashimoto, T. Kaneko, C. Rohrhofer, and K. Suzuki (JLQCD), Phys. Rev. D **103**, 074506 (2021), arXiv:2011.01499 [hep-lat].
- [34] S. Aoki, Y. Aoki, H. Fukaya, S. Hashimoto, C. Rohrhofer, and K. Suzuki (JLQCD), PTEP **2022**, 023B05 (2022), arXiv:2103.05954 [hep-lat].
- [35] T.-W. Chiu, PoS **LATTICE 2013**, 165 (2014).
- [36] M. I. Buchoff *et al.*, Phys. Rev. D **89**, 054514 (2014), arXiv:1309.4149 [hep-lat].
- [37] O. Kaczmarek, R. Shanker, and S. Sharma, Phys. Rev. D **108**, 094501 (2023), arXiv:2301.11610 [hep-lat].
- [38] A. Alexandru and I. Horváth, Phys. Rev. Lett. **127**, 052303 (2021), arXiv:2103.05607 [hep-lat].
- [39] A. Alexandru, I. Horváth, and N. Bhattacharyya, Phys. Rev. D **109**, 014501 (2024), arXiv:2310.03621 [hep-lat].
- [40] A. Alexandru, C. Bonanno, M. D'Elia, and I. Horváth, (2024), arXiv:2404.12298 [hep-lat].
- [41] H. Pandey, R. Shanker, and S. Sharma, (2024), arXiv:2407.09253 [hep-lat].
- [42] A. Alexandru and I. Horváth, Phys. Rev. D **92**, 045038 (2015), arXiv:1502.07732 [hep-lat].
- [43] A. Alexandru and I. Horváth, Phys. Rev. D **100**, 094507 (2019), arXiv:1906.08047 [hep-lat].
- [44] R. Bignell, G. Aarts, C. Allton, B. Jäger, S. Kim, J.-I. Skullerud, and A. Smecca, in *42th International Symposium on Lattice Field Theory* (2026) arXiv:2601.21178 [hep-lat].
- [45] T.-W. Chiu and T.-H. Hsieh, (2026), arXiv:2602.14811 [hep-lat].
- [46] H. T. Ding, S. T. Li, S. Mukherjee, A. Tomiya, X. D. Wang, and Y. Zhang, Phys. Rev. Lett. **126**, 082001 (2021), arXiv:2010.14836 [hep-lat].
- [47] T. G. Kovacs, Phys. Rev. Lett. **132**, 131902 (2024), arXiv:2311.04208 [hep-lat].
- [48] S. Borsanyi *et al.*, Nature **539**, 69 (2016), arXiv:1606.07494 [hep-lat].
- [49] C. Bonati, M. D'Elia, G. Martinelli, F. Negro, F. Sanfilippo, and A. Todaro, JHEP **11**, 170 (2018), arXiv:1807.07954 [hep-lat].
- [50] M. Giordano, S. D. Katz, T. G. Kovacs, and F. Pittler, JHEP **02**, 055 (2017), arXiv:1611.03284 [hep-lat].
- [51] R. Kehr, D. Smith, and L. von Smekal, (2023), arXiv:2304.13617 [hep-lat].
- [52] A. M. Garcia-Garcia and J. C. Osborn, Phys. Rev. D **75**, 034503 (2007), arXiv:hep-lat/0611019.
- [53] T. G. Kovacs and F. Pittler, Phys. Rev. Lett. **105**, 192001 (2010), arXiv:1006.1205 [hep-lat].
- [54] M. Giordano, T. G. Kovacs, and F. Pittler, Phys. Rev. Lett. **112**, 102002 (2014), arXiv:1312.1179 [hep-lat].
- [55] L. Ujfalusi, M. Giordano, F. Pittler, T. G. Kovács, and I. Varga, Phys. Rev. D **92**, 094513 (2015), arXiv:1507.02162 [cond-mat.dis-nn].
- [56] G. Cossu and S. Hashimoto, JHEP **06**, 056 (2016), arXiv:1604.00768 [hep-lat].
- [57] M. Giordano, T. G. Kovacs, and F. Pittler, (2026), arXiv:2602.10921 [hep-lat].
- [58] H. T. Ding *et al.* (HotQCD), Phys. Rev. Lett. **123**, 062002 (2019), arXiv:1903.04801 [hep-lat].
- [59] J. T. Edwards and D. J. Thouless, Journal of Physics C: Solid State Physics **5**, 807 (1972).
- [60] Z. Lin, *The Chiral and $U(1)_A$ Symmetries of the QCD Phase Transition using Chiral Lattice Fermions*, Ph.D. thesis, Columbia U. (2014).

- [61] T. Blum *et al.* (RBC, UKQCD), Phys. Rev. D **93**, 074505 (2016), arXiv:1411.7017 [hep-lat].
- [62] C. Jung (RBC, UKQCD), PoS **LATTICE2021**, 165 (2022).
- [63] T. Bhattacharya *et al.*, Phys. Rev. Lett. **113**, 082001 (2014), arXiv:1402.5175 [hep-lat].
- [64] T. Kalkreuter and H. Simma, Comput. Phys. Commun. **93**, 33 (1996), arXiv:hep-lat/9507023.
- [65] M. Lüscher, JHEP **08**, 071 (2010), [Erratum: JHEP 03, 092 (2014)], arXiv:1006.4518 [hep-lat].
- [66] A. Bazavov, N. Brambilla, H. T. Ding, P. Petreczky, H. P. Schadler, A. Vairo, and J. H. Weber, Phys. Rev. D **93**, 114502 (2016), arXiv:1603.06637 [hep-lat].
- [67] V. Oganesyan and D. A. Huse, Phys. Rev. B **75**, 155111 (2007).
- [68] Y. Y. Atas, E. Bogomolny, O. Giraud, and G. Roux, Phys. Rev. Lett. **110**, 084101 (2013).
- [69] O. Giraud, N. Macé, E. Vernier, and F. Alet, Phys. Rev. X **12**, 011006 (2022).
- [70] R. G. Edwards, U. M. Heller, J. E. Kiskis, and R. Narayanan, Phys. Rev. D **61**, 074504 (2000), arXiv:hep-lat/9910041.
- [71] M. Giordano and T. G. Kovacs, Universe **7**, 194 (2021), arXiv:2104.14388 [hep-lat].
- [72] E. Hofstetter and M. Schreiber, Phys. Rev. B **48**, 16979 (1993).
- [73] F. J. Dyson, J. Math. Phys. **3**, 1191 (1962).
- [74] C. M. Canali, Phys. Rev. B **53**, 3713 (1996).
- [75] V. Kravtsov and K. Muttalib, Physical review letters **79**, 1913 (1997).
- [76] H. Yan, Phys. Rev. E **111**, 054213 (2025).
- [77] N. Rosenzweig and C. E. Porter, Phys. Rev. **120**, 1698 (1960).
- [78] T. A. Brody, J. Flores, J. B. French, P. A. Mello, A. Pandey, and S. S. M. Wong, Rev. Mod. Phys. **53**, 385 (1981).
- [79] G. Lenz and F. Haake, Phys. Rev. Lett. **67**, 1 (1991).
- [80] V. K. B. Kota and S. Sumedha, Phys. Rev. E **60**, 3405 (1999).
- [81] S. Schierenberg, F. Bruckmann, and T. Wettig, Phys. Rev. E **85**, 061130 (2012), arXiv:1202.3925 [math-ph].
- [82] F. Bruckmann, T. G. Kovacs, and S. Schierenberg, Phys. Rev. D **84**, 034505 (2011), arXiv:1105.5336 [hep-lat].
- [83] M. Giordano, T. G. Kovacs, and F. Pittler, JHEP **04**, 112 (2015), arXiv:1502.02532 [hep-lat].
- [84] R. N. Larsen, S. Sharma, and E. Shuryak, Phys. Rev. D **105**, L071501 (2022), arXiv:2112.04537 [hep-lat].
- [85] R. N. Larsen, S. Sharma, and E. Shuryak, Phys. Lett. B **794**, 14 (2019), arXiv:1811.07914 [hep-lat].
- [86] R. N. Larsen, S. Sharma, and E. Shuryak, Phys. Rev. D **102**, 034501 (2020), arXiv:1912.09141 [hep-lat].
- [87] J.-P. Blaizot and M. A. Nowak, Phys. Rev. Lett. **101**, 102001 (2008), arXiv:0801.1859 [hep-th].
- [88] S. Guin, H. Pandey, and S. Sharma, Phys. Lett. B **866**, 139490 (2025), arXiv:2501.04397 [hep-lat].
- [89] D. Basko, I. Aleiner, and B. Altshuler, Annals of Physics **321**, 1126 (2006).
- [90] D. A. Abanin, E. Altman, I. Bloch, and M. Serbyn, Rev. Mod. Phys. **91**, 021001 (2019).
- [91] S. Bera, H. Schomerus, F. Heidrich-Meisner, and J. H. Bardarson, Phys. Rev. Lett. **115**, 046603 (2015).
- [92] A. Smith, J. Knolle, D. L. Kovrizhin, and R. Moessner, Phys. Rev. Lett. **118**, 266601 (2017).
- [93] J. H. Pixley, P. Goswami, and S. Das Sarma, Phys. Rev. Lett. **115**, 076601 (2015).
- [94] F. von Oppen, Phys. Rev. Lett. **73**, 798 (1994).
- [95] M. A. Clark, R. Babich, K. Barros, R. C. Brower, and C. Rebbi (QUDA), Comput. Phys. Commun. **181**, 1517 (2010), arXiv:0911.3191 [hep-lat].
- [96] C. Lehner, M. Bruno, D. Richtmann, M. Schlemmer, R. Lehner, D. Knüttel, T. Wurm, L. Jin, S. Bürger, A. Hackl, and A. Klein, “Grid Python Toolkit (GPT), 2024-10,” (2024).